

CrystEngComm

Accepted Manuscript



This is an *Accepted Manuscript*, which has been through the Royal Society of Chemistry peer review process and has been accepted for publication.

Accepted Manuscripts are published online shortly after acceptance, before technical editing, formatting and proof reading. Using this free service, authors can make their results available to the community, in citable form, before we publish the edited article. We will replace this *Accepted Manuscript* with the edited and formatted *Advance Article* as soon as it is available.

You can find more information about *Accepted Manuscripts* in the [Information for Authors](#).

Please note that technical editing may introduce minor changes to the text and/or graphics, which may alter content. The journal's standard [Terms & Conditions](#) and the [Ethical guidelines](#) still apply. In no event shall the Royal Society of Chemistry be held responsible for any errors or omissions in this *Accepted Manuscript* or any consequences arising from the use of any information it contains.

ARTICLE

Strengthening $N\cdots X$ halogen bonding *via* nitrogen substitution in the aromatic framework of halogen-substituted arylpyrazinamides

Cite this: DOI: 10.1039/x0xx00000x

Received 00th January ????,
Accepted 00th January ????

DOI: 10.1039/x0xx00000x

www.rsc.org/

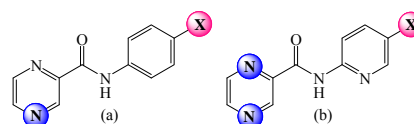
Hamid Reza Khavasi,* Mahdiah Hosseini, Alireza Azhdari Tehrani and Soheila Naderi

The importance of $N\cdots X$ halogen bonding in a series of *N*-(5-halo-2-pyridinyl)pyrazine-2-carboxamides has been investigated by different methods. The results show that when nitrogen is substituted for carbon in the aryl backbone of the parent compound, it can affect the electron accepting ability of bromine and iodine substituents. Thus, a stronger halogen bond can be formed.

Introduction

Weak non-covalent interactions play an important role in the self-assembly of molecules into supramolecular architectures. Among the non-covalent interactions, halogen bonding (XB) has attracted significant attention due to its potential applications in designing new solids with specific physical and chemical properties.¹ The term halogen bonding describes any non-covalent interaction involving halogens as electrophilic species. The interaction can be schematically described as $D\cdots X\cdots Y$, where X is the electrophilic halogen atom (XB donor), D is a donor of electron density (XB acceptor), and Y is a carbon, nitrogen or halogen atom.² It is well-known that the electron density is anisotropically distributed around the covalently bound halogen atom. As a result a region of the positive electrostatic potential (the so-called σ -hole) is formed on the outermost portion of the halogen's surface along the direction of the R–X bond, which concomitantly produces a perpendicular belt of negative electrostatic potential around the halogen. The positive character of the σ -hole increases down the group as the size and polarizability of the halogen increases, with a corresponding tendency for a halogen bond to become stronger.³

Many attempts have been made to enhance the electrophilicity of halogen atoms by substituting electron withdrawing groups, mostly fluorine⁴ atoms and rarely a nitro group,⁵ in the vicinity of the halogens. The attachment of halogen atom to a charged aromatic ring such as pyridinium^{6a,b} and pyrimidinium moiety,^{6c} also has been proposed as an alternative approach to polarize the halogen atom, thereby making it a better halogen bond donor. As part of our research interest in the study of weak intermolecular interactions⁷ and also halogen bonded systems,⁸ we became interested in exploring how the substituting of nitrogen for carbon in the aryl backbone of halogen-substituted phenylpyrazinamides could change the strength of halogen bonding and therefore affect the supramolecular structure. Thus in the



Scheme 1. *N*-(4-halophenyl)pyrazine-2-carboxamide, **X-phen** structures (a) and *N*-(5-halo-2-pyridinyl)pyrazine-2-carboxamide, **X-py** structures (b) the halogen bond donor and halogen bond acceptors are shown in purple and blue circles, respectively.

following, we present the crystal structures of *N*-(5-halo-2-pyridinyl)pyrazine-2-carboxamide, carrying different halogen atoms in the pyridine para-position to amide group. Compounds synthesized here can be schematically shown as **X-py**, where X shows the halogen atom, Scheme 1.

Results and Discussion

Synthesis. These compounds were prepared by modification of a method described previously.^{8b} Crystals suitable for X-ray analysis were obtained by slow evaporation of methanolic solution at room temperature. For comparing the halogen bonding geometrical parameters of **X-phen** and **X-py**, crystal structures of **X-phen** have been re-determined, at 298K, here, Table 1, Figure S1.^{8b}

Structural analysis of X-py compounds. X-ray crystallographic analyses reveal that **F-py**, **Br-py** and **I-py** crystallize in monoclinic $P2_1/n$ space group, while **Cl-py** crystallizes in the centrosymmetric triclinic space group $P\bar{1}$. ORTEP diagrams of compounds **X-py** drawn with 30% ellipsoid probability have been shown in Figure 1. The asymmetric unit of **F-py** consists of one crystallographically independent molecule, $Z'=1$. In **F-py**, discrete molecules are held together by head-to-tail $C_{pyz}\cdots H\cdots N_{py}$ hydrogen bonds for the generation of a dimeric unit, Figure 2(a), Table 2. Adjacent dimeric units are further linked to each other by $C_{py}\cdots F\cdots H\cdots C_{pyz}$

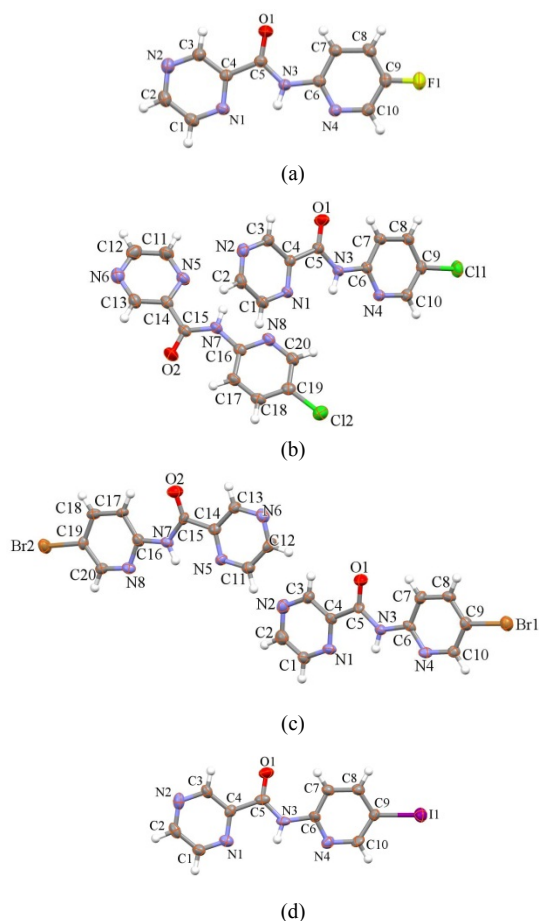


Figure 1. The ORTEP diagram of **F-py**, (a), **Cl-py**, (b), **Br-py**, (c) and **I-py**, (d), compounds. Ellipsoids are drawn at 30% probability level.

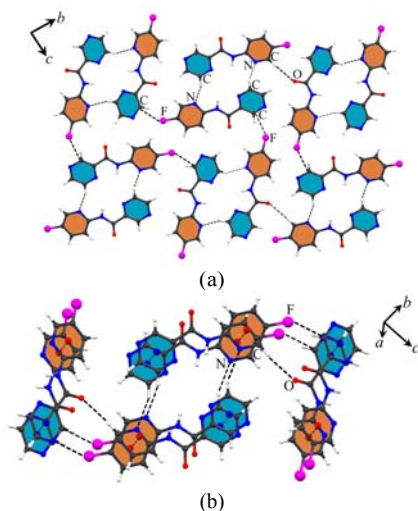


Figure 2. (a) A side view representation of *N*-(5-fluoro-2-yl)pyrazine-2-carboxamide, **F-py**, in *bc*-plane, showing the association of the adjacent molecules through head-to-tail $C_{\text{pyz}}\text{-H}\cdots\text{N}_{\text{py}}$ hydrogen bonds for the generation of a dimeric unit. Adjacent dimeric units are further linked to each other by $C_{\text{py}}\text{-F}\cdots\text{C}_{\text{pyz}}$ and $C_{\text{py}}\text{-H}\cdots\text{O}=\text{C}$ intermolecular interactions in *bc*-plane. (b) A side view representation of **F-py**, showing how extensive π - π stacking interactions, in *a*-direction, occur when the corresponding molecules are in parallel orientation with respect to one another to form an infinite one-dimensional tape.

and $C_{\text{py}}\text{-H}\cdots\text{O}=\text{C}$ intermolecular interactions in *bc*-plane. As Figure 2(b) shows, extensive π - π stacking interactions, in *a*-direction, also occur when the corresponding molecules are in parallel orientation with respect to one another to form an infinite one-dimensional tape, Table 3. Thus in **F-py**, the overall supramolecular structure is constructed by cooperation of π - π stacking, hydrogen bonds and $C_{\text{pyz}}\text{-F}\cdots\text{H}-C_{\text{pyz}}$ intermolecular interactions.

In **Cl-py** crystal packing, the most noticeable intermolecular features are $\text{C}=\text{O}\cdots\text{H}-C_{\text{pyz}}$, $C_{\text{pyz}}\text{-H}\cdots\text{N}_{\text{py}}$ and $C_{\text{py}}\text{-H}\cdots\text{Cl}$ hydrogen bonds, Table 2, that are cooperated with π - π stacking interactions between pyridine and pyrazine rings in *a*-direction, Figure 3, Table 3. Unlike in **Cl-phen**, the chlorine atom in **Cl-py** is not involved in any contacts that can be categorized as halogen bonds. The crystal structure of **Br-py** in the *bc*-plane is built up mainly by two kinds of $\text{N}\cdots\text{X}$ halogen bonds having different nitrogen atoms as halogen bond acceptors, ($\text{C}_9\text{-Br}_1\cdots\text{N}_6$ and $\text{C}_{19}\text{-Br}_2\cdots\text{N}_1$) and $\text{N-H}\cdots\text{Br}$ and $\text{C-H}\cdots\text{O}=\text{C}$ hydrogen bonds. A view of the crystal structure along the crystallographic *a*-axis reveals that $\pi_{\text{py}}\cdots\pi_{\text{pyz}}$ stacking interactions plays an important role in stabilizing the crystal structure, Figure 4, Tables 2 and 3. Based on the binding energies obtained from DFT calculations with correction for basis set superposition error (BSSE), of two $\text{N}\cdots\text{Br}$ halogen bonds, the stronger halogen bond is formed when the pyrazine nitrogen atom *anti* to the carbonyl is a halogen bond acceptor, for which the $\text{C-Br}\cdots\text{N}$ angle is farther from 180° but the $\text{C-Br}\cdots\text{N}$ distance is shorter, Table 4. In crystal packing of **I-py**, dimeric units are formed alternatively by head-to-tail $C_{\text{pyz}}\text{-H}\cdots\text{N}_{\text{py}}$ and $\text{C}=\text{O}\cdots\text{H}-C_{\text{py}}$ hydrogen bonds, in *a*-direction. Adjacent dimeric units are further linked to each other by head-to-tail $\text{N}\cdots\text{X}$ halogen bonds to generate a wave-like chain, Figure 5(a). Extensive $\pi_{\text{py}}\cdots\pi_{\text{pyz}}$ stacking interactions also stabilize the molecular packing in *c*-direction, Fig 5(b), Table 3.

Strengthening $\text{N}\cdots\text{X}$ halogen bonding via nitrogen substitution in the aromatic framework.

A comparison between significant intermolecular interactions controlling the packing of **X-phen** and **X-py** is illustrated in Scheme 2. A way to understand the strength of XB is considering and analyzing the crystal packing of isomolecular structures. This approach enables systematic investigation of crystal packing changes that arise as a consequence of tuning the relative strength of XB to the other interactions. Here, we report the crystallographic study of an isostructural **X-py** compounds, to provide new insights into the understanding of the effect of substituting the nitrogen for the CH group in the

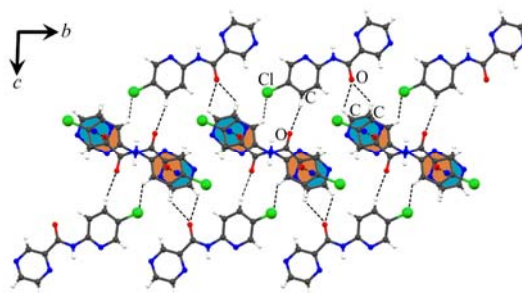


Figure 3. A side view representation of *N*-(5-chloro-2-yl)pyrazine-2-carboxamide, **Cl-py**, in *bc*-plane, showing the association of the adjacent molecules through $\text{C}=\text{O}\cdots\text{H}-C_{\text{pyz}}$, $C_{\text{pyz}}\text{-H}\cdots\text{N}_{\text{py}}$ and $C_{\text{py}}\text{-H}\cdots\text{Cl}$ hydrogen bonds that are cooperated with π - π stacking interactions between pyridine and pyrazine rings in *a*-direction.

Table 1. Structural data and refinement for compounds **F-py**, **Cl-py**, **Br-py**, **I-py**, **F-phen**, **Cl-phen**, **Br-phen** and **I-phen**.

	F-py	Cl-py	Br-py	I-py	F-phen	Cl-phen	Br-phen	I-phen
Formula	C ₁₀ H ₇ FN ₄ O	C ₁₀ H ₇ ClN ₄ O	C ₁₀ H ₇ BrN ₄ O	C ₁₀ H ₇ IN ₄ O	C ₁₁ H ₈ FN ₄ O	C ₁₁ H ₈ ClN ₄ O	C ₁₁ H ₈ BrN ₄ O	C ₁₁ H ₈ IN ₄ O
<i>f</i> _w	218.06	234.64	279.09	326.09	217.20	233.65	278.10	325.11
$\lambda/\text{\AA}$, <i>T/K</i>	0.71073, 298(2)	0.71073, 298(2)	0.71073, 298(2)	0.71073, 298(2)	0.71073, 298(2)	0.71073, 298(2)	0.71073, 298(2)	0.71073, 298(2)
Crystal system	Triclinic	Monoclinic	Monoclinic	Monoclinic	Monoclinic	Triclinic	Triclinic	Triclinic
<i>Z</i> , Space group	4, <i>P</i> ₂ ₁ / <i>n</i>	4, <i>P</i> ₁	8, <i>P</i> ₂ ₁ / <i>n</i>	4, <i>P</i> ₂ ₁ / <i>n</i>	8, <i>P</i> ₂ ₁ / <i>c</i>	2, <i>P</i> ₁	2, <i>P</i> ₁	2, <i>P</i> ₁
<i>a</i> // \AA	3.7671(5)	7.375(4)	7.287(2)	5.7717(3)	6.0141(15)	5.8988(19)	5.8743(6)	5.9550(8)
<i>b</i> // \AA	15.7465(19)	10.920(5)	24.367(5)	24.9374(8)	23.974(5)	7.408(3)	7.5065(7)	7.7126(11)
<i>c</i> // \AA	16.358(2)	13.606(7)	12.004(3)	7.5654(3)	13.582(3)	13.191(4)	13.3959(9)	12.9998(17)
$\alpha/^\circ$	90	86.20(4)	90	90	90	101.56(3)	101.489(7)	78.850(11)
$\beta/^\circ$	92.991(11)	83.56(4)	100.65(2)	94.819(4)	92.58(2)	96.55(2)	96.656(7)	85.640(11)
$\gamma/^\circ$	90	73.19(4)	90	90	90	110.55(3)	110.390(8)	70.594(11)
<i>V</i> / \AA^3 , <i>D</i> _{calc} /Mgcm ⁻³	969.0(2), 1.496	1041.6(9), 1.496	2094.7(9), 1.770	1085.5(8), 1.996	1956.2(8), 1.475	518.0(3), 1.498	531.44(8), 1.738	552.47(13), 1.954
<i>F</i> (000), 2 $\theta/^\circ$	448, 52.00	480, 58.64	1104, 52.00	624, 52.00	896, 58.44	240, 54.00	276, 52.00	312, 58.44
<i>R</i> (int), <i>S</i>	0.0599, 1.002	0.0657, 1.030	0.1256, 0.892	0.2180, 0.910	0.1016, 0.864	0.101, 1.038	0.0759, 0.998	0.0372, 1.091
<i>R</i> ₁ , <i>wR</i> ₂ (<i>I</i> > 2 σ (<i>I</i>))	0.0466, 0.0773	0.0710, 0.1168	0.0812, 0.1605	0.0787, 0.1239	0.0538, 0.0885	0.0715, 0.1410	0.0491, 0.1109	0.0296, 0.0668
CCDC No.	951201	951199	951197	951202	951200	951198	951196	877918

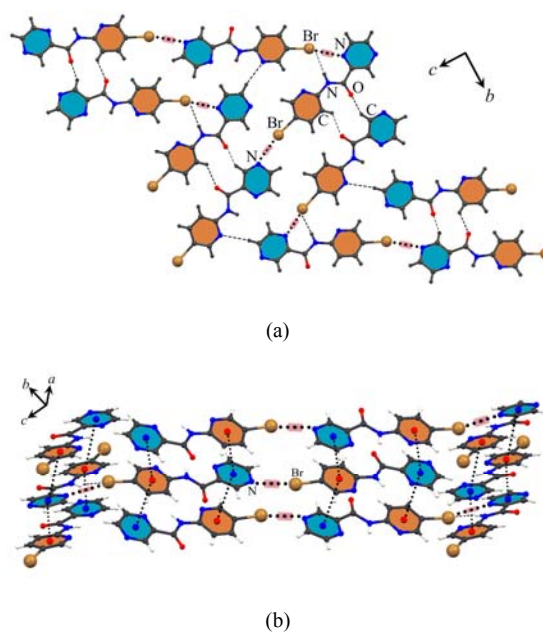


Figure 4. (a) A side view representation of *N*-(5-bromo-2-pyridinyl)pyrazine-2-carboxamide, **Br-py**, in *bc*-plane, showing the formation of a 2D sheet through N \cdots X halogen bonds, and N-H \cdots Br and C-H \cdots O=C hydrogen bonds. (b) A view of the **Br-py** crystal structure along the crystallographic *a*-axis, the $\pi_{\text{py}}\cdots\pi_{\text{pyz}}$ stacking interactions in an antiparallel fashion. Halogen bonds are highlighted in red.

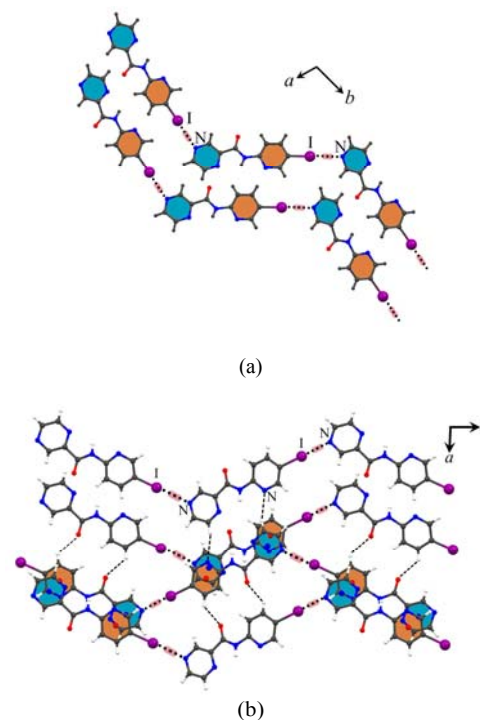


Figure 5. (a) A side view representation of *N*-(5-iodo-2-pyridinyl)pyrazine-2-carboxamide, **I-py**, in *ab*-plane, showing the formation of wave-like 1D chains through head-to-tail N \cdots I halogen bonds. (b) Generation of a dimeric unit in **I-py**, by head-to-tail C_{pyz}-H \cdots N_{py} and C=O \cdots H-C_{py} hydrogen bonds, in *a*-direction. Extensive $\pi_{\text{py}}\cdots\pi_{\text{pyz}}$ stacking interactions also stabilize the molecular packing in *c*-direction. Head-to-tail N \cdots I halogen bonds are highlighted in red.

Table 2. Selected hydrogen bond geometries for compounds **F-py**, **Cl-py**, **Br-py**, **I-py**, **F-phen**, **Cl-phen**, **Br-phen** and **I-phen**.

Compound	D-H...A	d(D-H)	d(H...A)	d(D...A)	<(DHA)
F-py	C10-H10...O1-C5 ^a	0.93	2.664	3.572(2)	175
	C1-H1...N4 _{py} ^b	0.93	2.619	3.495(3)	157
Cl-py	C1-H1...O2-C15 ^c	0.93	2.483	3.148(4)	129
	C18-H18...O1-C5 ^d	0.93	2.507	3.391(4)	159
	C2-H2...O2-C15 ^e	0.93	2.670	3.243(5)	121
	C10-H10...N2 _{pyz} ^f	0.93	2.687	3.594(4)	165
Br-py	C7-H7...Cl2-C19 ^g	0.93	2.964	3.689(4)	138
	C13-H13...O1-C5 ^h	0.93	2.449	3.26(1)	145
	C7-H7...O2-C15 ^h	0.93	2.625	3.28(1)	128
I-py	N3-H3B...Br2-C19 ^a	0.93	2.839	3.681(8)	166
	C8-H8...O1-C5 ⁱ	0.93	2.550	3.21(2)	128
F-phen	C1-H1...N4 _{py} ^j	0.93	2.640	3.54(2)	163
	C11-H11...O1-C5 ^k	0.93	2.453	3.293(3)	150
Cl-phen	C13-H13...N2 _{pyz} ^l	0.93	2.729	3.581(3)	153
	C19-H19...F1-C9 ^m	0.93	2.497	3.323(3)	148
	C8-H8...F2-C20 ^l	0.93	2.609	3.373(3)	140
	C11-H11...O1-C5 ^k	0.93	2.417	3.21(1)	143
Br-phen	C1-H1...N2 _{pyz} ^k	0.93	2.770	3.59(1)	148
	C3-H3...N1 _{pyz} ⁿ	0.93	2.779	3.61(1)	1149
	C11-H11...O1-C5 ⁿ	0.93	2.469	3.226(7)	139
I-phen	C1-H1...N2 _{pyz} ⁿ	0.93	2.764	3.592(8)	149
	C3-H3...N1 _{pyz} ^o	0.93	2.774	3.597(7)	148
	C7-H7...O1-C5 ⁿ	0.93	2.398	3.202(4)	145
	C1-H1...N2 _{pyz} ⁿ	0.93	2.841	3.677(5)	150

Symmetry codes: (a) $-1/2+x, 1/2-y, -1/2+z$, (b) $-x, 1-y, -z$, (c) $1-x, 1-y, 1-z$, (d) $x, y, 1+z$, (e) $1-x, 1-y, 1-z$, (f) $x, -1+y, z$, (g) $x, y, -1+z$, (h) $1-x, -y, 3-z$, (i) $-x, -y, 1-z$, (j) $2-x, -y, 2-z$, (k) $1+x, y, z$, (l) $1-x, -1/2+y, 3/2-z$, (m) $2-x, 1/2+y, 1.5-z$, (n) $-1+x, y, z$ and (o) $1+x, y, z$.

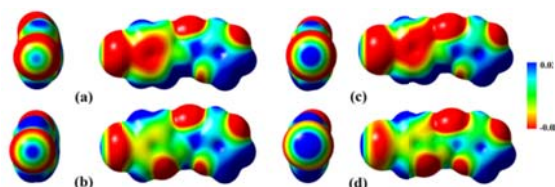
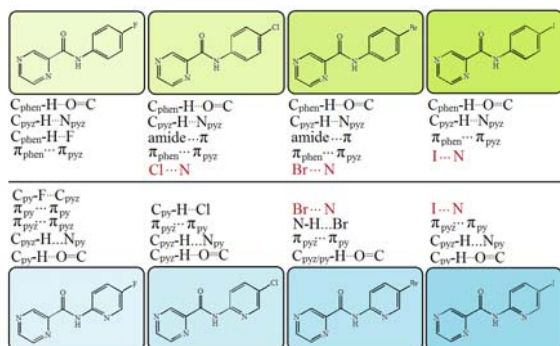


Figure 6. Electrostatic potentials mapped on the electron isodensity surface of **Br-phen** (a) **Br-py** (b) **I-phen** (c) and **I-py** (d) at the same contour value of 0.001 electron per Bohr³. The red color shows the most negative potential, while the blue color represents the most positive one. The side view representation of halogen σ -hole is shown on the left side of each MEP.



Scheme 2. A comparison between significant intermolecular interactions controlling the packing of **X-phen** and **X-py**.

aromatic backbone of series of compounds that have been recently investigated by us.^{8b} This effect has been studied recently by Blockhuys and his co-workers,⁹ who have investigated the factors influencing the activation and de-activation of fluorine synthons, in a different molecular system. The nitrogen atom is isoelectronic with a CH group; thus aromaticity is maintained when CH group(s) constituting the framework of the phenylpyrazinamide system is (are) replaced by the nitrogen atom(s), scheme 1. The nitrogen atom of the pyridine ring in the *N*-(5-halo-2-pyridinyl)pyrazine-2-carboxamide molecule, imports new features into the crystal engineering of phenylpyrazinamide derivatives. The pyridinic nitrogen atom either could be directly involved in new intermolecular interactions, such as C-H...N_{py} hydrogen bonds, or could indirectly alter the electron distribution of the aromatic ring, to which the halogen atom is bonded. The dihedral angles between the plane of pyrazine and pyridine rings lies between 1.24 and 4.34° for **X-py** compounds, Table 5. **X-py** compounds compared with **X-phen**, show better coplanarity between the aromatic rings, which is the consequence of intramolecular N-H...N_{py} hydrogen-bond formation. In addition to intramolecular hydrogen bonding, the pyridinic nitrogen atom is mainly involved in intermolecular C-H...N_{py} hydrogen bonds for the formation of dimeric units, Table 2. Investigation of intermolecular interactions and crystal packing of **F-py** and **Cl-py** via Hirshfeld surface analysis¹⁰ reveal that, upon the replacement of halogen-substituted phenyl group of phenylpyrazinamide by a halogen-substituted pyridine group, the probability of hydrogen bonding increases while that of π ... π stacking decreases, Figure S2. The differences in tendency of aromatic rings to stack *via* π -bonding can be elucidated through a comparison of molecular electrostatic potential surfaces of the **F-py** and **Cl-py** as shown in Figure S3. The presence of a nitrogen heteroatom within the ring changes the π -electron distribution throughout the carbon backbone, therefore, the aromatic ring in **X-py** becomes considerably electron poorer than in **X-phen**. As a result, the **Cl-py** exhibits crystal packing where hydrogen bonding interactions are favored over weak N...Cl halogen bonding, a type of bonding which has been observed in **Cl-phen** crystal packing. As expected, the halogen bond strength is enhanced by using a heavier halogen substituent. Accordingly, the interesting feature in crystal structures of **Br-py** and **I-py** is that there is a tendency to form halogen bonding synthon between halopyridyl and pyrazine rings. For **Br-phen**, **Br-py**, **I-phen** and **I-py**, the N...X distances of 3.284(5), 3.35(1) and 3.26(1), 3.450(3) and 3.11(1) Å, respectively, between halogen and nitrogen atoms are 3.4%, 1.4% and 4.1%, 2.2% and 11.9% shorter than the sum of the van der Waals radii, respectively, Table 4. The $\theta_{N...X-C}$ angle of the halogen bonded compounds investigated here varies between 154.0(3)° and 175.9(5)°, Table 4. The nearly linear geometry of N...X is in agreement with the $n \rightarrow \sigma^*$ character of this bonding interaction.^{1b,c} The stronger participation of the bromine atom in **Br-py**, compared with **Br-phen**, suggests that the pyridinic nitrogen exerts a polarizing effect on the halogen atom, thereby promoting larger σ -hole, Figure 6. This has been manifested in the higher proportion of halogen bonding interactions in **Br-py** (6.1%) relative to **Br-phen** (4.6%), Figure 7. In case of **I-py**, the pyridinic nitrogen atom induces a stronger polarizing effect to the halogen substituent, due to the higher polarizability of the iodine atom. Thus, the participation of iodine in N...X halogen bonding is approximately doubled on going from **I-phen** (3.1%) to **I-py** (6.0%).

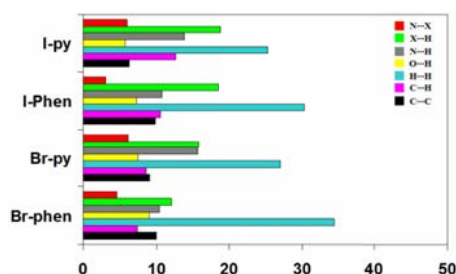
Table 3. π - π stacking interaction geometries for compounds **F-py**, **Cl-py**, **Br-py**, **I-py**, **F-phen**, **Cl-phen**, **Br-phen** and **I-phen**.

Complex	Interaction	Type of Interaction	C-C (Å)	P-P (°)	P-CC (°)
F-py	π - π Stacking	$\pi_{\text{pyz}}-\pi_{\text{pyz}}$, $\pi_{\text{py}}-\pi_{\text{py}}$	3.767	0.0	25.109, 26.302
Cl-py	π - π Stacking	$\pi_{\text{pyz}}-\pi_{\text{py}}$	3.849, 4.028	3.62	29.551, 28.316, 23.228, 26.252
Br-py	π - π Stacking	$\pi_{\text{pyz}}-\pi_{\text{py}}$	3.727, 3.739, 3.777, 3.805	3.6	19.831, 23.440, 23.877, 22.066
I-py	π - π Stacking	$\pi_{\text{pyz}}-\pi_{\text{py}}$	3.677, 3.977	4.34	22.299, 26.418, 29.306, 33.509
F-phen	π - π Stacking	$\pi_{\text{pyz}}-\pi_{\text{phen}}$	3.764, 3.842, 3.874, 3.785	7.89, 8.37, 8.55, 9.05	25.001, 18.379, 24.577, 18.471 23.454, 21.151, 22.926, 20.572
Cl-phen	π - π Stacking	$\pi_{\text{pyz}}-\pi_{\text{phen}}$	3.865	11.34	16.750, 20.125
	amide $\cdots\pi$	amide $\cdots\pi$	3.494	-	-
Br-phen	π - π Stacking	$\pi_{\text{pyz}}-\pi_{\text{phen}}$	3.904	11.05	19.058, 20.152
	amide $\cdots\pi$	amide $\cdots\pi$	3.534	-	-
I-phen	π - π Stacking	$\pi_{\text{pyz}}-\pi_{\text{phen}}$	3.747, 3.992	8.15	19.180, 13.065, 27.869, 22.429

It was of interest to investigate further, using theoretical methods, the halogen bonding energy in **Br-phen**, **Br-py**, **I-phen** and **I-py** compounds. The binding energies obtained from DFT calculation with correction for basis set superposition error (BSSE) on two relative fragments provide us an opportunity to evaluate the halogen bonding interaction energy between two fragments. The selected fragments were cut out directly from CIF data. The outcomes obtained from DFT methods are listed in Table 4. From these data, shown that $N\cdots X$ ($X=\text{Br}$ and I) halogen bonding energies vary within a range of -14.03 to -23.54 $\text{kJ}\cdot\text{mol}^{-1}$. The theoretical results show that the halogen bonding interaction energy increases moving from **Br-phen** to **Br-py** and from **I-phen** to **I-py**, Table 4. Interestingly enough, in the **X-phen** ($X=\text{Cl}$, Br , I) and **X-py** ($X=\text{Br}$, I) series, the melting points are increased by increasing the strength of halogen bonding interaction energies.

Conclusion

In conclusion, replacement of CH groups in **Br-Phen** and **I-phen** compounds by nitrogen atoms leads to crystal structures where the importance of halogen bonding becomes even more pronounced. Interestingly enough, in the **X-phen** ($X=\text{Cl}$, Br , I) and **X-py** ($X=\text{Br}$, I) series, the melting points are increased by increasing the strength of halogen bonding interaction energies. The results of this study should provide an additional design tool in crystal engineering to tune the relative strength of the halogen bonding.

**Figure 7.** Relative contributions of various intermolecular contacts to the Hirshfeld surface area in **Br-phen**, **Br-py**, **I-phen** and **I-py** Compounds

Experimental Section

Chemicals and instrumentation. All solvents such as methanol and pyridine and the chemicals were commercially available (reagent grade) and were purchased from Merck and Aldrich and used without further purification. Infrared spectra ($4000\text{--}400\text{ cm}^{-1}$) of solid samples were taken as 1% dispersion in KBr pellets using a BOMEM - MB102 spectrometer. ^1H NMR spectra were recorded on a Bruker AC-300 MHz spectrometer at ambient temperature in CD_3OD . All chemical shifts are quoted in part per million (ppm) relative to tetramethylsilane. Melting point was obtained by a Bamstead Electrothermal type 9200 melting point apparatus and corrected.

Synthesis of *N*-(5-halophenyl)-2-pyrazinecarboxamides, **X-phen.** The compounds **F-phen**, **Cl-phen**, **Br-phen** and **I-phen** were prepared by simply mixing the same equivalents of *para*-haloaniline and pyrazinecarboxylic acid in pyridine in the presence of triphenyl phosphite, according to what has been reported previously.^{8b}

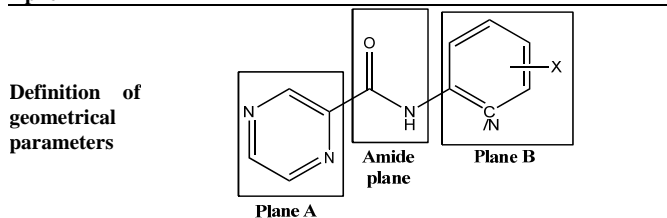
Synthesis of *N*-(5-fluoro-2-yl)pyrazine-2-carboxamide, **F-py.** The *N*-(5-fluoro-2-yl)pyrazine-2-carboxamide compounds were prepared by the reaction of 2-Amino-5-fluoropyridine (5 mmol) and pyrazine-2-carboxylic acid (5 mmol) in pyridine under the boiling point and in reflux condition. Specifically, 2-Amino-5-fluoropyridine (5 mmol) in 15 ml pyridine was added to a solution of pyrazine-2-carboxylic acid (5 mmol) in 15 ml pyridine. The resulting solution was stirred at 313 K for 20 min, then triphenyl phosphite (5 mmol) was added dropwise, and the reaction mixture was stirred 5 h at 373 K and 24 h

Table 4. Halogen Bond geometries and Calculated XB Binding Energies for **Br-phen**, **Br-py**, **I-phen** and **I-py** Compounds.

Compound	$X\cdots N(\text{Å})$	$C-X\cdots N(^{\circ})$	Reduction of the sum of the VDW radii (%)	Symmetry code	Calculated XB energy (kJ/mol)
X = Br					
Br-phen	3.284(5)	162.8(2)	3.4	-1+x, y, -1+z	-14.03
Br-py	3.35(1)	166.8(4)	1.4	1-x, -y, 2-z	-16.63
	3.26(1)	154.0(3)	4.1	1/2+x, 1/2-y, 1.5+z	-18.94
X = I					
I-phen	3.450(3)	166.66(9)	2.2	-1+x, 1+y, -1+z	-14.52
I-py	3.11(1)	175.9(5)	11.9	1/2-x, 1/2+y, 1.5-z	-23.54

Table 5. Dihedral angles between plane A, plane B and amide plane in **X-phen** and **X-py** compounds (plane A = pyrazine ring, plane B = phenyl or pyridyl ring).

Compound	∠ amide plane and plane A (°)	∠ amide plane and plane B (°)	∠ plane A and plane B (°)
F-py	3.45	2.13	1.24
Cl-py	2.62, 6.53	3.97, 2.93	3.26, 3.62
Br-py	5.60, 2.31	3.35, 1.70	3.52, 3.95
I-py	8.15	12.44	4.34
F-phen	4.17, 5.11	12.030, 14.16	7.89, 9.05
Cl-phen	0.52	11.38	11.34
Br-phen	0.96	12.00	11.05
I-phen	3.08	11.00	8.15



at ambient temperature. The mixture was added to 200 ml distilled water. Precipitation of a white solid resulted with a yield of 60%, which was filtered off and dried under reduced pressure. Upon slow evaporation of the filtrate at room temperature, suitable crystals of **F-py** for X-ray analysis were obtained after 6 days (melting point = 161 °C). Anal. calcd for $C_{10}H_7FN_4O$: C, 55.05; H, 3.23; N, 25.68. Found: C, 54.85; H, 3.14; N, 25.48. FT-IR (KBr pellet, cm^{-1}): 3339, 1944, 1844, 1696, 1577, 1543, 1398, 1229, 1102, 1014, 841, 769, 674, 534, 423. 1H NMR ($CDCl_3$, δ from TMS): 10.21 (1H-pyrazine), 9.50 (amidic H), 8.83 (1H-pyrazine), 8.62 (1H-pyrazine), 8.42-8.46 (1H-pyridine), 8.22 (1H-pyridine) and 7.49-7.55 (1H-pyridine).

Synthesis of *N*-(5-chloro-2-yl)pyrazine-2-carboxamide, **Cl-py**.

The procedure was similar to the synthesis of **F-py** except that 2-Amino-5-chloropyridine was used instead of 2-Amino-5-fluoropyridine. Precipitation of a white solid resulted with a yield of 70%, which was filtered off and dried under reduced pressure. Upon slow evaporation of the filtrate at room temperature, suitable crystals of **Cl-py** for X-ray analysis were obtained after 7 days (melting point = 165 °C). Anal. calcd for $C_{10}H_7ClN_4O$: C, 51.19; H, 3.01; N, 23.88. Found: C, 51.15; H, 2.95; N, 23.76. FT-IR (KBr pellet, cm^{-1}): 3352, 1957, 1698, 1572, 1523, 1462, 1380, 1301, 1100, 1016, 842, 736, 680, 438, 302. 1H NMR ($CDCl_3$, δ from TMS): 10.23 (1H-pyrazine), 9.51 (amidic H), 8.84 (1H-pyrazine), 8.63 (1H-pyrazine), 8.40-8.43 (1H-pyridine), 8.33 (1H-pyridine), 7.74-7.78 (1H-pyridine).

Synthesis of *N*-(5-bromo-2-yl)pyrazine-2-carboxamide, **Br-py**.

The procedure was similar to the synthesis of **F-py** except that 2-Amino-5-bromopyridine was used instead of 2-Amino-5-fluoropyridine. Precipitation of a white solid resulted with a yield of 55%, which was filtered off and dried under reduced pressure. Upon slow evaporation of the filtrate at room temperature, suitable crystals of **Br-py** for X-ray analysis were obtained after 8 days (melting point = 166 °C). Anal. calcd for $C_{10}H_7BrN_4O$: C, 43.03; H, 2.53; N, 20.07. Found: C, 42.97; H, 2.45; N, 19.72. FT-IR (KBr pellet, cm^{-1}): 3339, 1900, 1823, 1700, 1570, 1525, 1356, 1283, 1087, 1035, 829, 776, 663, 502, 438. 1H NMR ($CDCl_3$, δ from TMS): 10.22 (1H-pyrazine), 9.51 (amidic H), 8.84 (1H-pyrazine), 8.63 (1H-pyrazine), 8.50-8.53 (1H-pyridine), 8.35-8.42 (1H-pyridine) and 7.87-7.9 (1H-pyridine).

Synthesis of *N*-(5-iodo-2-yl)pyrazine-2-carboxamide, **I-py.** The procedure was similar to the synthesis of **F-py** except that 2-Amino-5-iodopyridine was used instead of 2-Amino-5-fluoropyridine. Precipitation of a white solid resulted with a yield of 70%, which was filtered off and dried under reduced pressure. Upon slow evaporation of the filtrate at room temperature, suitable crystals of **I-py** for X-ray analysis were obtained after 8 days (melting point = 170 °C). Anal. calcd for $C_{10}H_7IN_4O$: C, 36.83; H, 2.16; N, 17.18. Found: C, 36.80; H, 2.14; N, 17.13. FT-IR (KBr pellet, cm^{-1}): 3352, 1690, 1563, 1530, 1356, 1290, 989, 842, 660, 522, 441, 275. 1H NMR ($CDCl_3$, δ from TMS): 10.18 (1H-pyrazine), 9.49 (amidic H), 8.83 (1H-pyrazine), 8.62 (1H-pyrazine), 8.55 (1H-pyridine), 8.24-8.27 (1H-pyridine) and 8.02-8.05 (1H-pyridine).

Single crystal diffraction studies. For all compounds apart from **F-phen** the intensity data were collected on a STOE IPDS-II or STOE-IPDS-2T diffractometers with graphite monochromated Mo-K α radiation, 0.71073 Å. Data were collected at a temperature of 298(2) K in a series of ω scans in 1° oscillations and integrated using the Stoe X-AREA¹¹ software package. A numerical absorption correction was applied using X-RED¹² and X-SHAPE¹³ software's. The X-ray data for compound **F-phen** was collected using a Bruker SMART APEX-II CCD diffractometer equipped with fine focus 1.75 kW sealed tube Mo-K α radiation, 0.71073 (Å). The total number of images was based on the results from the program COSMO.¹⁴ Cell parameters were retrieved using the APEX II software¹⁵ and refined using SAINT on all observed reflections. Data reduction was performed using the SAINT software,¹⁶ which corrects for Lorentz and Polarizing effects. Scaling and absorption corrections were applied using the SADABS¹⁷ multi-scan technique, supplied by George Sheldrick. All the structures were solved by direct methods using SHELXS-97 and refined with full-matrix least-squares on F^2 using the SHELXL-97 program package¹⁸ All non-hydrogen atoms were refined anisotropically. Hydrogen atoms were added at ideal positions and constrained to ride on their parent atoms, with Uiso(H) = 1.2Ueq. All the refinements were performed using the X-STEP32 crystallographic software package.¹⁹ Structural illustrations have been drawn with MERCURY²⁰ windows. ORTEP diagrams of these complexes are shown in Figures 1 and S1. Crystallographic details including crystal data and structure refinement are listed in Table S1.

Computational Details. DFT calculations were performed using the ORCA quantum chemistry suite.²¹ The local spin density approximation (LSD) exchange correlation potential was used with the local density approximation of the correlation energy.²² Gradient-corrected geometry optimizations²³ were performed by using the generalized gradient approximation (Perdew–Wang non-local exchange and correlation corrections–PW91).²⁴ The selected two fragments were cut out directly from the CIF data without optimization. Large atom basis sets TZP are used to ascribe all the atoms here. A frozen core approximation was used to treat the core electrons: (1s) for C and N, (4p) for I, (3p) for Br, (2p) for Cl, (1s) for O and F. Scalar relativistic effects were taken into account by using the zeroth-order regular approximation (ZORA).²⁵

Computational details for generating molecular Electrostatic potential surface. Electrostatic potential surfaces were generated for **F-phen**, **F-py**, **Cl-phen**, **Cl-py**, **Br-phen**, **Br-py**, **I-phen** and **I-py** from DFT calculations performed at the B3LYP/6-311G (d,p) basis set for all atoms except iodine, and the LANL2DZdp-ECP (with polarization functions of d symmetry and diffuse functions of p symmetry) basis set for iodine. Potential surfaces were mapped by

conventional molecular electron density (0.001 electron/ Bohr³) and color-coding.

Acknowledgements

We would like to thank the Graduate Study Councils of Shahid Beheshti University, General Campus and Iran National Elite Foundation for financial support.

Notes and references

^aFaculty of Chemistry, Shahid Beheshti University, G. C., Evin, Tehran 1983963113, Iran. E-mail: h-khavasi@sbu.ac.ir; Fax: +98 21 22431663

†Electronic Supplementary Information (ESI) available: ORTEP diagrams of X-phen compounds, electrostatic potentials mapped on the electron isodensity surface of **F-phen**, **Cl-phen**, **F-py** and **Cl-py**, relative contributions of various intermolecular contacts to the Hirshfeld surface area in **F-phen**, **F-py**, **Cl-phen** and **Cl-py** and full crystallographic data (CCDC No. 951196-951202 and 877918). These materials available free of charge via the Internet at <http://pubs.rsc.org>.

- (1) (a) Metrangolo, P.; Resnati, G. *Cryst. Growth Des.* 2012, 12, 5835–5838. (b) Pennington, W. T.; Resnati, G.; Taylor, M. S. *CrystEngComm*, 2013, 15, 3057–3057. (c) Metrangolo, G.; Resnati, G. *Halogen Bonding: Fundamentals and Applications*; Springer: Berlin, 2008. (d) Meazza, L.; Marti-Rujas, J.; Terraneo, G.; Castiglioni, C.; Milani, A.; Pilati, T.; Metrangolo, P.; Resnati, G. *CrystEngComm*, 2011, 13, 4427–4435 (e) Raatikainen, K.; Rissanen, K. *Chem. Sci.*, 2012, 3, 1235. (f) Marti-Rujas, J.; Colombo, L.; Lü, J.; Dey, A.; Terraneo, L.; Metrangolo, P.; Pilati, T.; Resnati, G. *Chem. Commun.*, 2012, 48, 8207–8209. (g) Marti-Rujas, J.; Meazza, L.; Keat Lim, G.; Terraneo, L.; Pilati, T.; D. M. Harris, K.; Metrangolo, P.; Resnati, G. *Angew. Chem. Int. Ed.*, 2013, 52, 13444–13448.
- (2) (a) Metrangolo, P.; Neukirch, H.; Pilati, T.; Resnati, G. *Acc. Chem. Res.* 2005, 38, 386–395. (b) Metrangolo, P.; Meyer, F.; Pilati, T.; Resnati, G.; Terraneo, G. *Angew. Chem., Int. Ed.* 2008, 47, 6114–6121.
- (3) Politzer, P.; Murray, J. S. *ChemPhysChem*. 2013, 14, 278.
- (4) (a) Roper, L. C.; Präsang, C.; Kozhevnikov, V. N.; Whitwood, A. C.; Karadakov, P. B.; Bruce, D. W. *Cryst. Growth Des.* 2010, 10, 3710–3720. (b) Präsang, C.; Whitwood, A. C.; Bruce, D. W. *Cryst. Growth Des.* 2009, 9, 5319–5326. (c) Valerio, G.; Raos, G.; Mielle, S. V.; Metrangolo, P.; Resnati, G. *J. Phys. Chem. A*, 2000, 104, 1617–1620.
- (5) K. Raatikainen, K.; Rissanen, K. *CrystEngComm*, 2009, 11, 750–752. (b) Garden, S. J.; da Cunha, F. R.; Wardell, J. L.; Skakle, J. M. S.; Low, J. N.; Glidewell, C. *Acta Crystallogr., Sect. C: Cryst. Struct. Commun.*, 2002, 58, 463–465.
- (6) (a) Logothetis, T. A.; Meyer, F.; Metrangolo, P.; Pilati, T.; Resnati, G. *New J. Chem.*, 2004, 28, 760–763. (b) K. Raatikainen, K.; Cametti, M.; Rissanen, K. *Beilstein J. Org. Chem.*, 2010, 6, 4. (c) Riley, K. E.; Murray, J. S.; Politzer, P.; Concha, M. C.; Hobza, P. J. *Chem. Theory Comput.*, 2009, 5, 155.
- (7) (a) Khavasi, H. R.; Mir Mohammad Sadegh, B. *Cryst. Growth Des.*, 2012, 12, 4798–4804. (b) Khavasi, H. R.; Azizpoor Fard, M. *Cryst. Growth Des.* 2010, 10, 1892–1896. (c) Khavasi, H. R.; Salimi, A. R.; Eshtiahi-Hosseini, H.; Amini, M. M. *CrystEngComm* 2011, 13, 3710–3717.
- (8) Khavasi, H. R.; Azhdari Tehrani, A. *Inorg. Chem.*, 2013, 52, 2891–2905. (b) Khavasi, H. R.; Azhdari Tehrani, A. *CrystEngComm*, 2013, 15, 3222–3235.
- (9) Collas, A.; De Borger, R.; Amanova, T.; Blockhuys, F. *CrystEngComm*, 2011, 13, 702–710.
- (10) McKinnon, J. J.; Spackman, M. A.; Mitchell, A. S.; *Acta Cryst.* 2004, B60, 627–668. (b) Spackman, M. A.; McKinnon, J. J.; *CrystEngComm*. 2002, 4, 378–392. (c) Wolff, S. K.; Grimwood, D. J.; McKinnon, J. J.; Turner, M. J.; Jayatilaka, D.; Spackman, M. A. *CrystalExplorer 3.0*; University of Western Australia: Perth, Australia, 2012.
- (11) *X-AREA*, version 1.30, program for the acquisition and analysis of data, Stoe & Cie GmbH: Darmstadt, Germany, 2005.
- (12) *X-RED*, version 1.28b, program for data reduction and absorption correction, Stoe & Cie GmbH: Darmstadt, Germany, 2005.
- (13) *X-SHAPE*, version 2.05, program for crystal optimization for numerical absorption correction, Stoe & Cie GmbH: Darmstadt, Germany, 2004.
- (14) COSMO V1.58, *Software for the CCD Detector Systems for Determining DataCollection Parameters*. Bruker Analytical X-ray Systems, Madison, WI (2008).
- (15) APEX2 V2008.5-0 *Software for the CCD Detector System*; Bruker Analytical X-ray Systems, Madison, WI (2008).
- (16) SAINT V 7.34 *Software for the Integration of CCD Detector System* Bruker Analytical X-ray Systems, Madison, WI (2008).
- (17) SADABS V2.008/2 Program for absorption corrections using Bruker-AXS CCD based on the method of Robert Blessing; Blessing, R.H. *Acta Cryst. A* 51, 1995, 33–38.
- (18) Sheldrick, G. M. *SHELX97*, program for crystal structure solution and refinement, University of Göttingen, Göttingen, Germany, 1997.
- (19) *X-STEP32*, version 1.07b, crystallographic package, Stoe & Cie GmbH: Darmstadt, Germany, 2000.
- (20) Mercury 3.1 Supplied with Cambridge Structural Database; CCDC: Cambridge, U.K., 2003–2004.
- (21) Neese, F.; Becker, U.; Ganyushin, D.; Liakos, D. G.; Kossmann, S.; Petrenko, T.; Riplinger, C.; Wennmohs, F. *ORCA, 2.7.0*; University of Bonn: Bonn, 2009.
- (22) Vosko, S. H.; Wilk, L.; Nusair, M. *Can. J. Phys.*, 1980, 58, 1200.
- (23) (a) Versluis, L.; Ziegler, T. *J. Chem. Phys.*, 1988, 88, 322; (b) Fan, L.; Ziegler, T. *J. Chem. Phys.*, 1991, 95, 7401.
- (24) Perdew, J. P.; Chevary, J. A.; Vosko, S. H.; Jackson, K. A.; Pederson, M. R.; Singh, D. J.; Fiolhais, C. *Phys. Rev.*, 1992, 46, 6671.
- (25) van Lenthe, E.; Baerends, E. J.; Snijders, J. G. *J. Chem. Phys.*, 1993, 99, 4597; (b) van Lenthe, E.; Baerends, E. J.; Snijders, J. G.; *J. Chem. Phys.*, 1994, 101, 9783; (c) van Lenthe, E.; van Leeuwen, R.; Baerends, E. J.; Snijders, J. G. *Int. J. Quantum Chem.*, 1996, 57, 281.

Graphical abstract

